



UNIVERSIDADE ESTADUAL DE CAMPINAS
SISTEMA DE BIBLIOTECAS DA UNICAMP
REPOSITÓRIO DA PRODUÇÃO CIENTÍFICA E INTELLECTUAL DA UNICAMP

Versão do arquivo anexado / Version of attached file:

Versão do Editor / Published Version

Mais informações no site da editora / Further information on publisher's website:

<https://www.sciencedirect.com/science/article/pii/S0260877423000869>

DOI: <https://doi.org/10.1016/j.jfoodeng.2023.111488>

Direitos autorais / Publisher's copyright statement:

©2023 by Elsevier. All rights reserved.

DIRETORIA DE TRATAMENTO DA INFORMAÇÃO

Cidade Universitária Zeferino Vaz Barão Geraldo

CEP 13083-970 – Campinas SP

Fone: (19) 3521-6493

<http://www.repositorio.unicamp.br>



Encapsulation of resveratrol via spray-drying of oil-in-water emulsions produced by ultrasound or membrane emulsification

Larissa Consoli^{a,*}, Míriam Dupas Hubinger^b, Marijana M. Dragosavac^c

^a Centre of Natural Sciences, Federal University of São Carlos – Buri, São Paulo, Brazil

^b School of Food Engineering, University of Campinas – Campinas, São Paulo, Brazil

^c Department of Chemical Engineering, Loughborough University – Loughborough, Leicestershire, United Kingdom

ARTICLE INFO

Keywords:

Resveratrol
Microencapsulation
Membrane emulsification
Spray drying
Energy density

ABSTRACT

Resveratrol emulsions do not have long shelf life hence drying to obtain powder can result in the resveratrol protection, shelf life extension and can unlock versatile applications in food, pharmaceuticals, and cosmetics. In this work resveratrol was emulsified using drop-by-drop (“batch” and “continuous” membrane) and classic (ultrasound) emulsification methods followed by the emulsion spray drying to obtain resveratrol loaded microparticles. Influence of the emulsification techniques on the microparticles properties, resveratrol encapsulation efficiency and retention were evaluated and the energy density required by each emulsification process was estimated. 10 and 15 μm pore membranes produced droplets between 154 and 42 μm , while with the ultrasound droplets of 0.16 μm were produced. The microparticles obtained by spray-drying of the emulsions produced by ultrasound and “batch membrane system” had the highest encapsulation (~97%) efficiency and similar resveratrol retention (~89%). This confirms that membrane systems (even producing larger droplet size compared to ultrasound emulsions) could achieve high encapsulation efficiency and resveratrol retention. Since no cooling is needed during membrane emulsification due to the low energy input, membrane systems with their ability to be scaled up, should be considered in food and pharma as an alternative to classical emulsification systems especially when shear and heat sensitive compounds are emulsified and encapsulated.

1. Introduction

Resveratrol (3,4',5-trihydroxystilbene) is a phenolic compound naturally found in food sources such as grapes, blueberries and peanuts. It has been recognized to have antioxidant, anti-inflammatory, anti-diabetics, anti-obesity, anticarcinogenic and cardioprotective effects. Despite these beneficial properties, it has a limited use in edible, pharmaceutical and cosmetic formulations due to poor stability and low bioavailability caused by factors such as its low water solubility, low oxidative stability and photosensitivity (Santos et al., 2019). Therefore, there is a great drive to encapsulate it within protective materials to improve the solubility and stability.

To deal with the limitations commonly associated with the poor stability and low bioavailability of resveratrol, many encapsulation techniques have been employed. Some of them include spray drying (Consoli et al., 2020, 2019), complex coacervation and entrapment in protein polysaccharide complexes (Zhang et al., 2021). Particularly, the increased oil solubility of resveratrol in comparison to aqueous systems

(Consoli et al., 2020) makes oil-in-water emulsions effective carriers for this compound.

There are several emulsification methods based on droplet disruption or individual droplet formation. Droplet disruption methods usually employ mechanical devices of high-energy requirement, such as rotor-stator/high-pressure homogenizers, microfluidizers, and ultrasonic probes (Sneha and Kumar, 2022). The latter has been receiving great interest for applications in food products, due to its ability to produce kinetically stable emulsions of small droplet size (from nano-to micro-scale) with a fast (process usually demands few minutes) and easy-cleaning operation (Taha et al., 2020). However, sonication can increase the temperature of the materials during its application, which might lead to thermal degradation of heat sensitive compounds. Membrane emulsification stands out as a made-to-measure method, where droplets are formed individually when the dispersed phase is forced through a porous membrane into the continuous phase. It is a low-energy process, which provides a more accurate control over droplet size and enables the production of monodispersed emulsions (Yu

* Corresponding author.

E-mail address: larissa.consoli@ufscar.br (L. Consoli).

<https://doi.org/10.1016/j.jfoodeng.2023.111488>

Received 14 November 2022; Received in revised form 21 February 2023; Accepted 23 February 2023

Available online 25 February 2023

0260-8774/© 2023 Elsevier Ltd. All rights reserved.

et al., 2022). Since low fluxes ($0.01\text{--}0.1\text{ m}^3\text{ (m}^2\text{h)}^{-1}$) are usually employed in batch membrane devices (Vladisavljević and Williams, 2005), scaling up to pilot units using metal membranes, where fluxes of up to $5.7\text{ m}^3\text{ (m}^2\text{h)}^{-1}$ may be reached (Holdich et al., 2020) represent an interesting alternative enabling the production of larger batches in shorter periods. To produce a 100 L batch, this change from lab scale to pilot scale can provide a reduction in the processing time from about 1 h (flux of $0.1\text{ m}^3\text{ (m}^2\text{h)}^{-1}$) to 1 min (flux of $5.7\text{ m}^3\text{ (m}^2\text{h)}^{-1}$), considering the same membrane area.

Regardless of the technique used to produce the emulsions, the energy requirement of the process is always a concerning point, especially if there is any expectation for scaling-up (Schubert and Engel, 2004). In this sense, the energy density is a concept that relates the power introduced into a mechanical device to the volume flow rate when it is producing emulsions (Karbstein and Schubert, 1995). The energy density gives valuable information regarding the design of emulsification processes and enables the comparison between different emulsification methods when energy densities of the same order of magnitude are employed (Santos and Cunha, 2020).

The use of oil-in-water emulsions as resveratrol carriers may not represent the most convenient formulation since the high-water content usually brings down the shelf life to a few weeks if no preservatives are employed. Furthermore, increased water content demands bigger volume for storage and impacts the transportation costs. As an alternative, the spray drying technique is frequently associated as a downstream process to convert an emulsion into a powder form which stability can be extended to a couple of years, storage footprint is decreased as well as the transportation costs (Assadpour and Jafari, 2019). Some of the properties of the spray-dried powders, including particle size, encapsulation efficiency and the ability to reconstitute emulsions are influenced by the feed liquid characteristics (concentration, viscosity, density, surface tension, and solvent boiling point) (Salama, 2020). Therefore, controlling the properties of the emulsions is an important factor when it is intended to use them as vehicles for bioactive compounds. Such control is directly connected to the emulsification method employed.

Our research group has recently combined a lab scale membrane device with the spray drying technique to produce resveratrol-loaded microparticles, obtaining high encapsulation efficiencies (Consoli et al., 2020). In this work, we extended the study and have evaluated the energy densities of high (ultrasound) and low energy (membrane systems) emulsification affects the properties of emulsion and spray-dried resveratrol-loaded microparticles.

2. Materials and methods

2.1. Material

The continuous phases were composed of sodium caseinate (90.7 g protein/100 g on dry weight basis, Alibra Ingredients - Campinas, SP, Brazil), Maltodextrin MOR-REX 1910 (M10 - Dextrose Equivalent (DE) = 9–12) and Dried Glucose Syrup (DGS) MOR-REX 1930 (DE = 26–30), both supplied by Ingredion Brazil Industrial Ingredients Ltd. (Mogi-Guaçu, SP, Brazil). Refined sunflower oil (SFO) was purchased from a local shop. Resveratrol (98% purity), used in the formulations, was a donation from Naturex (São Paulo, SP, Brazil). Resveratrol HPLC grade ($\geq 99\%$ purity), Nile red dye and Sodium azide ($\geq 99.5\%$ purity) were supplied by Sigma Aldrich Company Ltd. (Gillingham, Dorset, UK). Ethanol (95% v/v - Fisher Chemical), Acetonitrile (HPLC grade - Fisher Chemical), formic acid (99% LC/MS grade - Fisher Chemical) were purchased from Fisher Scientific (Loughborough, Leicestershire, UK).

2.2. Experimental procedure

Experiments were divided into three main stages. In stage one, Nile red dyed emulsions were prepared to set the operational conditions in the membrane systems. In stage two, resveratrol-loaded emulsions were

produced in the membrane systems by using those conditions established in stage one, and also by using an ultrasound equipment with operational conditions from a previous work (Consoli et al., 2017). In stage three, resveratrol-loaded emulsions were spray-dried and powder characterization was performed.

2.2.1. Dispersions preparation

Individual dispersions of sodium caseinate (14.0 g/100 g dispersion), maltodextrin (49.4 g/100 g dispersion) and dried glucose syrup (DGS) (49.4 g/100 g dispersion) were prepared by using Milli-Q water containing 0.01% sodium azide (antimicrobial agent). The dispersions were stirred overnight using magnetic stirrers, at room temperature. Then, the three dispersions were mixed to reach a total solid concentration of 26.8 g/100 g, with the mass proportion between sodium caseinate/M10/DGS kept at 1/1/1. The pH of the mixture was adjusted to 7.5 using 1 M NaOH. This aqueous mixture was used to set the best membrane emulsification process conditions and will be referred to as “the control mixture” in the next parts of the work. The control mixture was used to produce protein-polysaccharide conjugates (the “Maillard-reacted mixture”) via the Maillard reaction, using a wet-heating method described in a former work (Consoli et al., 2020). Briefly, 500 g of the control mixture was poured into a Schott Duran® bottle and sealed. The container was kept in a water bath at 75 °C, where it was gently stirred manually to ensure homogenization every hour. After 6 h, the bottle was removed from the hot water and then soaked in an ice bath to cease the reaction. Before being employed to produce the emulsions, the pH of this mixture was adjusted to 7.5 using 1 M NaOH, at room temperature. Detailed information regarding the composition of emulsions is provided in Table 1.

2.2.2. Membrane emulsification

A Dispersion Cell system (Micropore Technologies, Wilton Centre, UK), which will be further referred to as “batch system”, was first used to prepare the emulsions. It consisted of a lab scale equipment composed of a glass cylinder, where the continuous phase was placed within, and a disk membrane (d_m) situated at the bottom of the glass cylinder. The membrane had nominal pore diameter $D_{p,dm} = 10\text{ }\mu\text{m}$, porosity $\epsilon_{dm} = 1.046\%$ and useful surface area $A_{dm} = 0.000908\text{ m}^2$, calculated neglecting gasket diameter. The continuous phase was kept under stirring using a paddle blade stirrer positioned on the top of the glass cylinder and coupled to a DC power supply (Kenwood PA36-3A), which would control the rotational speed hence providing the shear stress for droplet formation on the membrane surface. The dispersed phase was forced through the disk membrane and injected into the continuous phase by a syringe pump (WPI-World Precision Instruments Inc., AL-1000, UK). The feed rate was kept at 1.0 mL min^{-1} , resulting in a flux of $66.1\text{ L h}^{-1}\text{ m}^{-2}$ through the membrane. The Nile red-dyed emulsions were firstly used to determine operational conditions. The rotational speed was evaluated at 200, 575, 950, 1300 and 1650 rpm, resulting in average shear stresses of 0.1, 1.5, 6.5, 15.3 and 28.9 Pa over the membrane surface, respectively. Nile red was used to enable the visualization

Table 1

Formulations of the emulsions produced using membrane emulsification and ultrasound devices.

Emulsions formulations ^a	Continuous phase ^b (95.5 g/100 g emulsion)	Dispersed phase (4.5 g/100 g emulsion)
Nile-red dyed emulsions	Control mixture: sodium caseinate, M10, DGS; pH 7.5	Sunflower oil + Nile red (0.002 g/100 g oil)
Resveratrol-loaded emulsions	Maillard-reacted mixture* pH 7.5	Sunflower oil + ethanol (1 mL/50 mg resveratrol) + resveratrol (20 mg/100 g emulsion)

^a Both formulations had 30 g/100 g of total solids to favour the spray drying process.

^b Viscosity = 108,4 mPa s; density = 1.108 kg/m³.

of the oil phase injection into the control mixture, which was opaque due to the presence of sodium caseinate. Prior to emulsification, the Nile red dye was added to sunflower oil and solubilized using magnetic stirring for about 1 h. Resveratrol-loaded emulsions were produced using the process conditions established after evaluating the results obtained from the Nile red dyed emulsions. Ethanol was used to solubilize resveratrol under magnetic stirring for 2 min. This solution was then added to sunflower oil and this mixture was kept under agitation for 1 min, using a magnetic stirrer.

Mathematical modelling was used to predict the droplet size of emulsions produced by the membrane systems. The applied calculation was based on a force balance on the membrane pore (Dragosavac et al., 2008; Kosvintsev et al., 2005). Two models were derived from Equation (1). Model I used the average shear stress on the membrane surface, whilst Model II used the maximum shear stress. For detailed calculations of shear stress and droplet predicted size, please check the Supplementary Material.

$$D = \frac{\sqrt{18\tau^2 r_p^2 + 2\sqrt{81\tau^4 r_p^4 + 4r_p^2 \tau^2 Y^2}}}{3\tau} \quad 1$$

Where D is the predicted droplet diameter; τ is the shear stress on the membrane surface; $r_p = d_p/2$ is the membrane pore radius ($d_p/2$) and Y is the interfacial tension between the disperse and continuous phases, which was equal to 10.8 mNm^{-1} for the control mixture/Nile red-dyed SFO, as determined using the pendant drop method as previously described by Consoli et al. (2020).

As for the continuous membrane (cm) emulsification process, a Torsional System (Micropore Technologies, North Yorkshire, UK) was employed. In this equipment, droplets detachment from the membrane surface occurred both by the crossflow of the continuous phase and by the oscillating axial movement of the cylindrical membrane. A tubular stainless-steel membrane ($D_{p,cm} = 15 \mu\text{m}$; $\varepsilon_{cm} = 0.44\%$; $A_{cm} = 0.0052 \text{ m}^2$) was used. This membrane was assembled concentrically to the cylindrical unit through which the continuous phase would flow. The dispersed phase was injected into the membrane from the top, using a syringe pump (WPI-World Precision Instruments Inc., AL-1000, UK), at a feed rate of 5.75 mLmin^{-1} , which was determined to provide the cylindrical membrane the same dispersed phase flux that was employed to the disk membrane of the batch system, considering the difference in the surface area of both membranes. The dispersed phase flowed radially into the external part of the membrane, where the continuous phase was flowing from the bottom to the top, as it was pushed by a peristaltic pump 313S (Watson Marlow Fluid Technology Group, Cornwall, UK) at a flow rate of $109.25 \text{ mLmin}^{-1}$. This flow rate was calculated to produce emulsions with the same oil phase concentration ($4.5 \text{ g oil phase}/100 \text{ g emulsion}$) as used in the “batch system”. The frequency of operation at which the membrane would be moved was controlled, and so was the displacement of the membrane around its own axis. To determine the most suitable operation conditions to our system, the experiments were performed at 15 and 30 Hz (maximum reached by the equipment was 50 Hz), using both 2 and 5 mm of displacement, using the Nile Red-dyed formulation. The resveratrol-loaded emulsions were produced using the set conditions. The experiments were performed twice in each tested condition. During “batch” and “continuous” membrane emulsification overheating of the formed emulsion was not observed and temperature of the emulsion stayed constant ($20 \text{ }^\circ\text{C}$) hence no cooling was required. In both membrane emulsification systems, membrane cleaning was performed after each assay. The membranes (disk or cylindrical) were cleaned as previously described by Consoli et al. (2020) as recommended by the manufacturer (Micropore Technologies, Winton Centre, UK).

2.2.3. Ultrasound emulsification

This stage of the work was performed for a comparison purpose using

operational conditions established in a former work for a similar formulation (Consoli et al., 2017). Only resveratrol-loaded emulsions were produced. Firstly, a coarse emulsion was prepared ($300 \text{ g}-285 \text{ mL}$). The oil phase, which was composed of the mixture of sunflower with ethanol-solubilized resveratrol, was added to the Maillard-reacted continuous phase and stirred at $20,000 \text{ rpm}$ for 2 min using a rotor-stator device (Ultra-Turrax T18 basic, Ika-Werke GmbH & Co. kg, Staufen, Germany). Then, a sonication probe (Branson Digital Sonifier S450-D – frequency 20 kHz , full power 400 W , Danbury, CT, USA) was immersed 3 cm within the centre of the beaker (half of the liquid height), and the fine emulsions were obtained after sonication for 7 min using 100% of power amplitude. During the ultrasound emulsification the temperature of the emulsion could have increased to $100 \text{ }^\circ\text{C}$ within the 7 min as observed in previous experiments. Therefore, to avoid the sample overheating, the beaker with the emulsion was kept inside an ice bath during the sonication process.

2.2.4. Emulsions characterization

Droplet size of emulsions was determined using laser diffraction in a Mastersizer 2000 (Malvern Instruments Ltd., Malvern, UK). D_{50} represents the diameter of cumulative distribution of 50% of total droplets and was used to express the mean droplet diameter (Dragosavac et al., 2008). Droplet size polydispersity was expressed as the Span (Eq. (2)). The distilled water at room temperature was used as the dispersant medium during analysis.

$$Span = \frac{(D_{90} - D_{10})}{D_{50}} \quad 2$$

where D_{10} , D_{50} , and D_{90} represent the diameter of cumulative distribution of 10% , 50% and 90% of total droplets, respectively.

Emulsion microstructure was observed using an optical microscope GT Vision FXM-L3201 (GT Vision Ltd., Stansfield, UK) coupled to a QImaging digital camera (QImaging Ltd, Surrey, Canada), with $100\times$ or $200\times$ magnification. The software QCapture Suite 2.98.2 was used for image acquisition.

2.2.5. Spray drying process and microparticles characterization

Immediately after emulsions production, they were fed into the atomizing nozzle ($D_{nozzle} = 0.5 \text{ mm}$) of a lab scale SD06 Spray Dryer (Labplant UK Ltd, Hunmanby, UK). The feed rate of 10 mLmin^{-1} was controlled using the peristaltic pump coupled to the equipment. The drying air flow rate was $30 \text{ m}^3\text{h}^{-1}$ and the inlet temperature was kept at $180 \text{ }^\circ\text{C}$, based on a previous works reporting on sodium caseinate spray drying (Drusch et al., 2009). The outlet temperature was recorded to be $98.2 \pm 4.6 \text{ }^\circ\text{C}$. The compressed air was operated at a flow rate of $2 \text{ m}^3\text{h}^{-1}$ ($2-4 \text{ bar}$). The assays were performed in duplicate whereas the powder characterization analyses were made at least in triplicate.

Microparticle water content was determined using a gravimetric method in which 0.600 g of the sample was placed in a drying oven at $105 \text{ }^\circ\text{C}$ until reaching constant weight (after 24 h) (AOAC, 2005).

The particle size was determined using laser light scattering as described in section 2.2.6.1, using the De Brouckere diameter $D_{4,3}$ (Eq. (3)) to express mean particle size and ethanol 99.5% purity as dispersant medium.

$$D_{4,3} = \frac{\sum n_i D_i^4}{\sum n_i D_i^3} \quad 3$$

Where n_i is the number of droplets with diameter D_i .

The morphology of the microparticles was evaluated using Scanning Electron Microscopy (SEM). The spray-dried powders were covered with a metal layer composed of 80% Gold and 20% Palladium, using a Q150-T Turbo-Pumped Sputter Coater (Quorum Technologies, Laughton, East Sussex, UK). Then, powders were fixed on the surface of metal stubs with carbon tapes. A Tabletop Scanning Electron Microscope (SEM) TM3030 (Hitach High-Technologies Corporation, Krefeld, Germany) with an

energy dispersive X-ray detector was used. Images were captured at 1,000x and 3,000× magnifications.

To evaluate the reconstituted emulsions, 0.6 g of powder was placed in plastic tubes and 5 mL of distilled water was added, following a manual stirring until the complete dissolution of the powder (Drapala et al., 2017). In the sequence, the droplet size and optical microscopy analyses were performed as described in section 2.2.6.

The quantification of resveratrol in the microparticles was performed using HPLC analysis, according to the methodology previously used by our research group (Consoli et al., 2020). The total amount of resveratrol in the particles was determined by a sequential dilution of the samples in an aqueous 75% acetonitrile solution followed by centrifugation and filtration into glass vials using syringe polyethersulfone (PES) filters of 0.22 μm (Millex®GP Millipore Express, Merck Millipore Ltd, Tullagreen, Ireland). The resveratrol content on the particles surface was obtained by mixing the samples with ethanol 99.5%, in the proportion 1/10 (mass particles/ethanol volume) followed by filtration using syringe filters. Samples were kept frozen until the HPLC analysis. 10 μL of the samples prepared as just described were injected in a reversed phase C18 column (Kinetex 5 μm, 100 × 4.60 mm, Phenomenex, Macclesfield, UK) coupled in an Agilent 1100 series (Agilent Technologies, Santa Clara, USA) liquid chromatograph equipped with a diode array detector (DAD G1315B). The analyzes were performed at 25 °C, in a flow rate of 0.8 mLmin⁻¹. A linear solvent gradient was applied as follows: 0–2 min: 60% of solvent A (milliQ water/formic acid, 99.8/0.2) and 40% of solvent B (acetonitrile, 100%); 5 min: 42% A and 58% B; 7 min: 60% A and 40% B. The wavelength was monitored at 306 nm. The resveratrol concentration was determined using calibration curves that were prepared in each batch of analyses, using standard solutions of concentration from 3 to 15 mgL⁻¹.

Resveratrol retention was defined as the ratio between the total amount of resveratrol (RSV) quantified in the microparticles by HPLC analysis and the total amount weighed into the formulations, as expressed by Eq. (4) (Consoli et al., 2020).

$$RR[\%] = \frac{\text{total RSV}_{HPLC}}{\text{total RSV}_{weighed}} \times 100 \quad 4$$

The ratio between the amount of resveratrol entrapped within the particle (and not on the surface) and the total amount quantified in the particles was defined as the encapsulation efficiency (Eq. (5)) (Consoli et al., 2020):

$$EE[\%] = \frac{(\text{total RSV}_{HPLC} - \text{superficial RSV}_{HPLC})}{\text{total RSV}_{HPLC}} \times 100 \quad 5$$

2.2.6. Energy density calculations

Energy density (ED) is an important factor to be considered when working on emulsification processes (Schubert and Engel, 2004). In our work, three emulsification methods were employed using the same formulation, each one with a particular calculation mode.

The total ED for the ultrasound emulsification is given by the sum of the ED delivered by the rotor-stator device and by the sonication equipment. When batch operations are performed, Eq. (6) can be applied for ED (J m⁻³) calculations in each one of these devices (Jafari et al., 2007):

$$ED = (P \times t) / V \quad 6$$

Where P is the power delivered to system (W); t is the time employed (s), and V is the volume of the fluid (m³), which was 285 mL (2.85 × 10⁻⁴ m³) in our system.

Karbstein and Schubert (1995) derived the equation to estimate the droplet size ($D_{3,2}$) as a function of the ED for the ultrasound emulsification ($D_{3,2} = C/ED^b$). Where C is the constant dependent on the dispersed phase viscosity and b is the empirical constant. According the equation smaller droplets can be produced when high ED is applied, and larger droplets can be produced when low ED is applied.

The rotor-stator device used in this work (details in section 2.2.5) had power consumption of 500 W according to the manufacturer specification data. As for the ultrasound system, the power was given by Eq. (7):

$$P = A \times FP \quad 7$$

Where A is the power amplitude used in the experiment (%) and FP represents the full power of the equipment (W), which was equal to 400 W in the sonicator used in this work (details in section 2.2.5).

Regarding the “batch membrane” emulsification, there was power consumption from the syringe pump and from the paddle blade stirrer which was used to move the continuous phase over the membrane surface. Eq. (8) was used to calculate the power consumption of these equipment:

$$P = U \times i \quad 8$$

Where P is the power delivered to system (W), U is the electric tension (V- Volts) and i is the electric current (A – Ampère).

The electric current was given by the manufacturer manual in the case of the syringe pump (0.75 A), for full load operation, and was displayed by the DC power supply for each voltage applied (0.29 A at 15 V).

As for the continuous membrane system, apart from its nominal power consumption (maximum 480 W, as given by the manufacturer manual), there was the one coming from the syringe pump used for the dispersed phase injection (same for the “batch system”) and the one consumed by the peristaltic pump used to move the continuous phase (maximum 100 W, given by the manufacturer). Since it is a continuous operation device, a 5 min operation process was fixed for the calculation using Equation (5), which corresponded to the production of 300 mL of emulsion.

2.3. Statistical analysis

Results were statistically analyzed by Tukey test, where differences between means were considered at a 5% significance level ($p \leq 0.05$) as performed in our previous work (Consoli et al., 2020). The analyses were performed using Microsoft Excel (2016 version).

3. Results and discussion

3.1. The effect of shear stress on the Nile Red-dyed emulsions produced by the “batch system”

The size parameters of emulsions are presented as a function of shear stress in Fig. 1.

Membrane emulsification process is affected by many factors concerning the formulation (phases viscosity and density), the membrane characteristics (material, pore size and porosity) and process parameters (shear stress, transmembrane pressure, flow rate, temperature) (Spyropoulos et al., 2011). In this study, since formulation, membrane and dispersed phase flux were fixed, the only factor responsible for shear stress variation over the membrane surface was the rotational speed, which was a controlled parameter. In Fig. 1A, the reduction caused to droplets diameter upon the increase on the shear stress can be noticed. Shear stress affects droplet detachment as it decreases the droplet formation time. Higher shear stresses corroborate to increase the drag forces over the droplets, which implies in the decrease of droplet size (Dragosavac et al., 2008). Droplet polydispersity was also reduced upon increased shear stresses, as shown by the Span (Fig. 1B).

The experimental data plotted in Fig. 1A were closer to the predicted droplet sizes of Models I and II when higher rotational speeds were used, in particular the predicted values from Model I. Model I is based on the average shear stress that is applied over the membrane surface, and thus simulates a situation closer to the actual process (as the full membrane

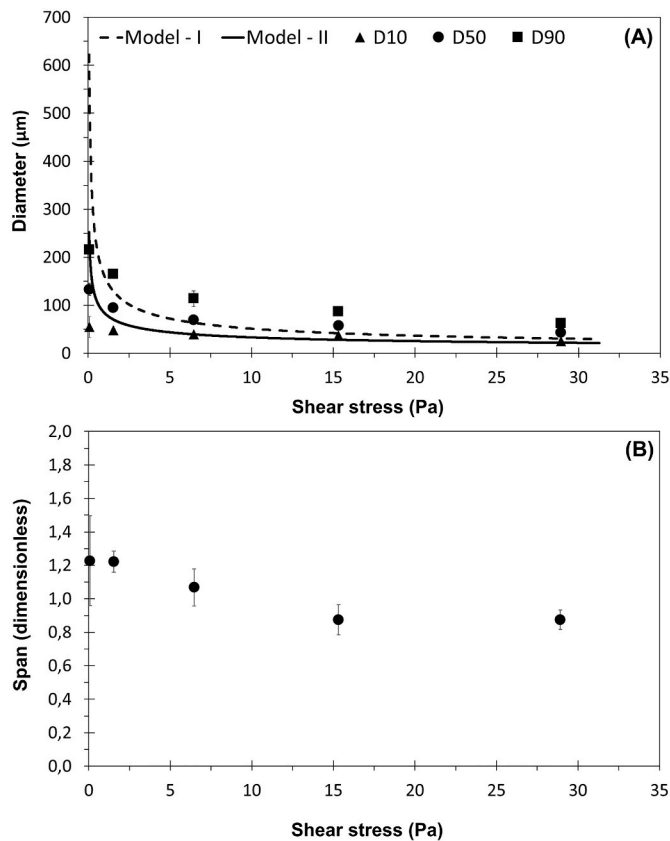


Fig. 1. (A) Diameter and (B) Span of Nile red-dyed emulsions produced using the Batch system, as a function of shear stress. Process was carried out using a feed rate of 1 mLmin⁻¹ (~66.1 Lh⁻¹m⁻²).

was used) than Model II, which considers the maximum shear stress occurring only on the critical radius. The distance of the predicted values obtained for both models at low shear stresses can be explained by the

fact that neither of the models considers the necking effect on droplet formation. At such low shear stresses, however, it should not be neglected (Dragosavac et al., 2008), and for this reason the noticeable difference between experimental and predicted values were reported.

The size distribution charts for the emulsions upon shear stress variation, and their respective micrographs are presented in Fig. 2. The chart highlights the narrower size distribution obtained at higher shear stresses over the membrane surface, as it had been suggested by the reduction on Span (Fig. 1B). The micrographs illustrate the sharp reduction of droplet when the average shear stress over the membrane surface was increased from 0.1 to 28.9 Pa. Furthermore, tighter size distribution can be observed in the micrographs in Fig. 2. Given such results, the highest average shear stress (28.9 Pa) was set to produce resveratrol-loaded emulsions.

3.2. Membrane emulsification using the “continuous system”

The “continuous system” represents a scaled-up process for the “batch system”. The total emulsion output rate was 115 mLmin⁻¹. The process parameters affecting the emulsions characteristics were evaluated to determine the most suitable condition to produce resveratrol-loaded emulsions and the results are shown in Table 2. Emulsions size distribution charts and their respective micrographs for each process condition are presented in Fig. 3. As can be seen in Fig. 3, the small peaks around 0.1, 1.0 and 10 μm were all attributed to the continuous phase, probably due to the presence of non-solubilized protein. The micrographs in Fig. 3 corroborates to this hypothesis, since none of the images showed evidence of such small droplets in the emulsion. For this reason, the size parameters presented in Table 2 consider only the main peak of the size distribution charts in Fig. 3.

Both frequency and membrane displacement caused variations in droplet diameter and polydispersity, though the effect caused by the displacement was stronger. At constant frequency, increasing the displacement caused significant reduction in droplet size. Albeit the statistics do not show a significant difference, increasing the frequency at constant displacement decreased droplet size, as evidenced by the micrographs in Fig. 4. Silva et al. (2015), when working with a similar continuous membrane system, reported that the main factor influencing

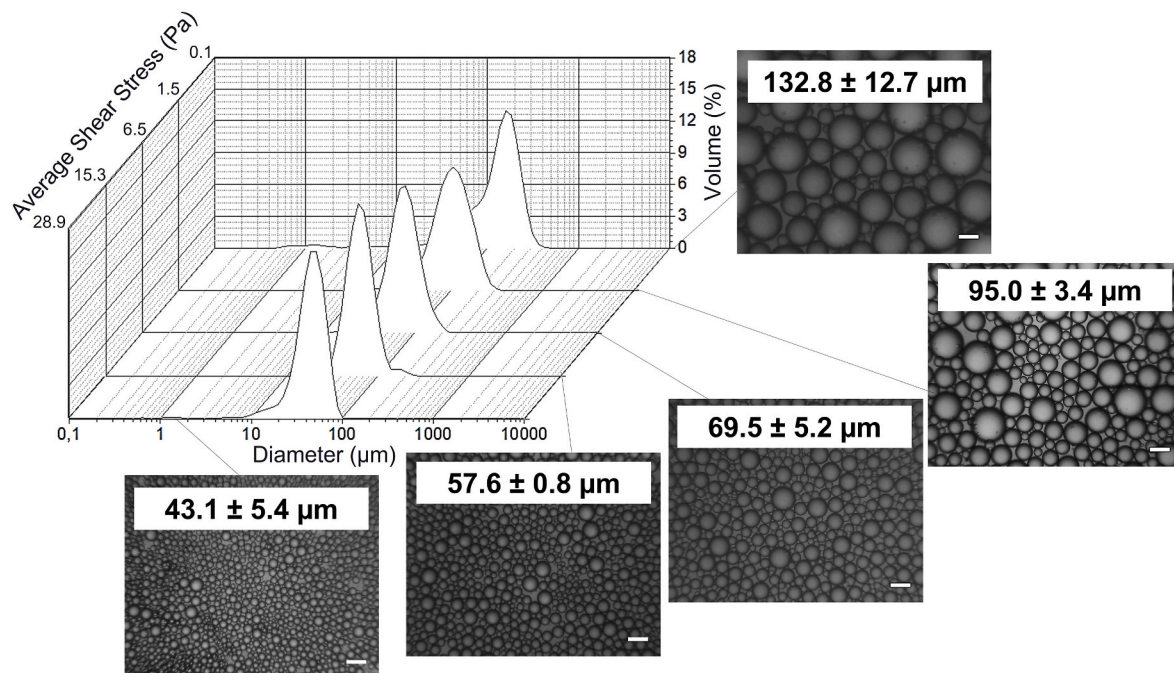


Fig. 2. Size distribution charts and micrographs of Nile red-dyed emulsions obtained using the Batch system, as a function of shear stress. The number in the micrographs represents D₅₀ of the correspondent emulsion. All emulsions were produced using 1 mLmin⁻¹ feed rate (~66.1 Lh⁻¹m⁻²). Scale bar: 100 μm.

Table 2
Size parameters of Nile red-dyed emulsions produced using the Torsional System, at different process conditions.

Frequency (Hz)	Displacement (mm)	Corresponding shear stress (Pa)	D ₁₀ (μm)	D ₅₀ (μm)	D ₉₀ (μm)	Span (dimensionless)
15	2	10	52.54 ± 13.50 ^a	119.64 ± 15.91 ^c	221.33 ± 23.25 ^c	1.42 ± 0.11 ^a
	5	25	45.97 ± 2.72 ^a	84.90 ± 1.94 ^{ab}	147.11 ± 3.37 ^b	1.19 ± 0.02 ^a
30	2	28	49.52 ± 0.75 ^a	89.16 ± 1.79 ^{bc}	154.10 ± 2.28 ^b	1.17 ± 0.01 ^a
	5	70	32.99 ± 4.33 ^a	54.99 ± 2.65 ^a	88.51 ± 15.10 ^a	1.00 ± 0.30 ^a

Different lowercase letters in the same column represent statistically significant difference ($p < 0.05$).

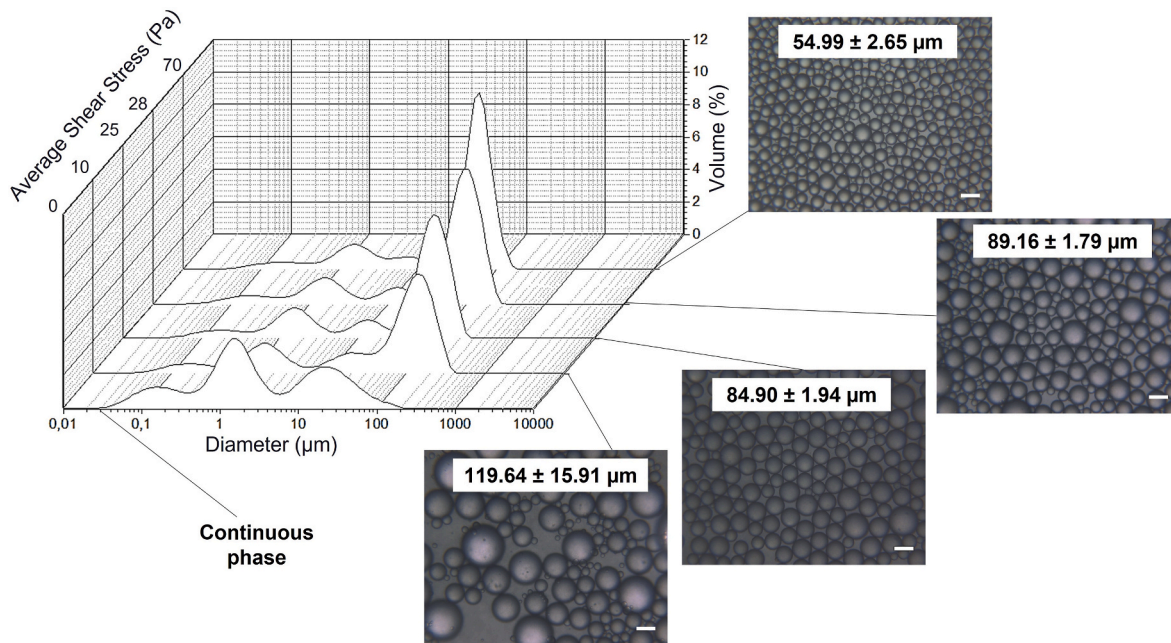


Fig. 3. Size distribution charts and micrographs of Nile red-dyed emulsions produced by the torsional system. Additional information regarding size parameters can be seen in Table 2. Emulsions were obtained at a dispersed phase feed rate of 5.75 mLmin⁻¹ and a continuous phase flow rate of 109.25 mLmin⁻¹. Scale bar: 100 μm.

the droplet size is the total shear stress on the membrane surface, independent of the combination of process parameters that generated it. Furthermore, the authors observed that droplet size uniformity depends on parameters other than shear stress, including frequency and membrane displacement, individually.

The condition of 30 Hz frequency and 5 mm of membrane displacement (shear stress of 70 Pa) produced emulsions with the smallest mean diameter ($54.99 \pm 2.67 \mu\text{m}$) and the most narrow size distribution (Span = 1.00 ± 0.30). This diameter is statistically comparable ($p < 0.05$) to that obtained for the Nile red-dyed emulsions produced using the “batch system” ($43.1 \pm 5.4 \mu\text{m}$) at the set process conditions. These results show that, even with the bigger pore size ($D_{p,cm} = 15 \mu\text{m}$) a membrane than the membrane used in the “batch system” ($D_{p,dm} = 10 \mu\text{m}$), the “continuous system” was able to produce emulsions of similar droplet sizes, and therefore can be considered an efficient scaling up alternative for the lab-scale membrane process.

3.3. A comparison between different emulsification processes

3.3.1. Resveratrol-loaded emulsions

Once process conditions were set for the “batch system” and for the “continuous system” using the Nile red-dyed emulsions, they were employed to produce resveratrol-loaded emulsions. For comparison purposes, ultrasound was employed to produce emulsions with the same formulation. Table 3 shows the size parameters for the resveratrol-loaded emulsions obtained in these three emulsification processes.

As it had occurred to the Nile red-dyed emulsions, the mean droplet size (D_{50}) of the “continuous system” emulsions was statistically similar

($p < 0.05$) to those from the “batch system”, despite the former having a slightly higher value. On the other hand, the ultrasound emulsions presented mean droplet size quite smaller than the other two processes ($D_{50} \sim 0.15 \mu\text{m}$). The obtention of droplets smaller than $0.10 \mu\text{m}$, as indicated by the D_{10} parameter, due to the necessity of safety studies before the application of the product, due to the potential cytotoxicity that can be presented by particles in this size range (Li et al., 2017; Pereira et al., 2013; Tibolla et al., 2018).

Differently from the membrane process, where each droplet is formed individually, in the sonication process the oil droplets are broken down from bigger to smaller ones once the acoustic cavitation phenomena is induced by the ultrasound waves generated by the system (Taha et al., 2020). For this reason, the mean droplet size that can be reached is usually smaller, whereas the polydispersity is expected to be high, because the acoustic cavitation does not reach all the droplets in the system uniformly (Jafari et al., 2007). Indeed, the Span of the sonicated resveratrol-loaded emulsions was about 2.75 times higher than that of the “batch system” emulsions, though very similar to that of the “continuous system”. Data in Table 3 also shows that size variability of emulsions produced by the Continuous system was higher in comparison to that of the emulsions obtained by the other methods, given their increased standard variations in D_{10} , D_{50} and D_{90} parameters. The droplet size distribution and micrographs obtained for the resveratrol-loaded emulsions of each process are presented in Fig. 4.

3.3.2. Spray-dried microparticles

The type of emulsification process affected powder characteristics with respect to size and resveratrol retention, as shown in Table 3. The

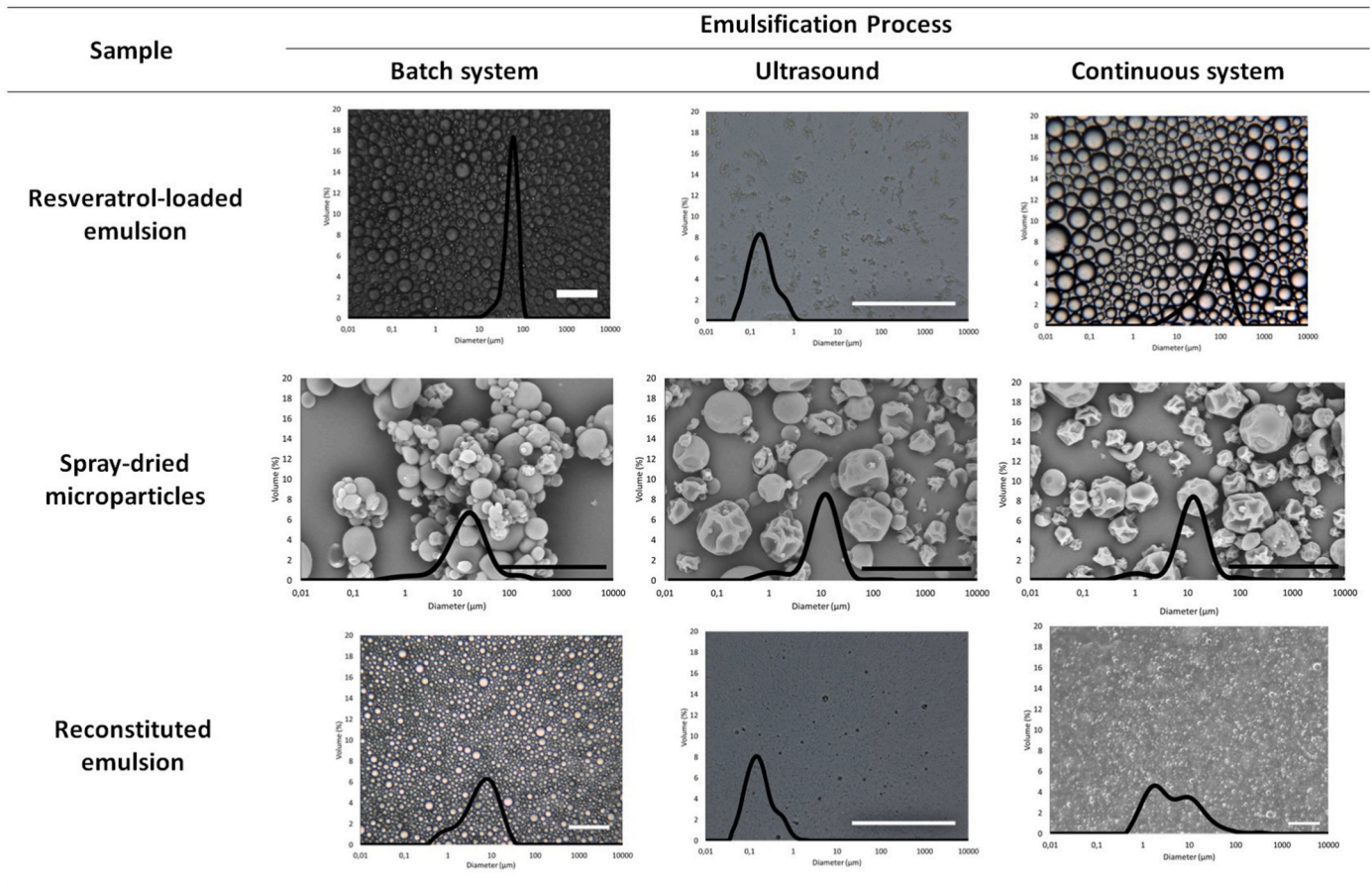


Fig. 4. Micrographs for the resveratrol-loaded emulsions, spray-dried microparticles and reconstituted emulsions obtained from each emulsification process. Scale bars are equal to 100 μm for the resveratrol-loaded and reconstituted emulsions, and 25 μm for the spray-dried microparticles. The difference in the scale bar sizes are a result of the different magnifications needed to visualize each sample.

microparticles obtained from the “batch system” emulsions had larger diameter ($D_{4,3}$) than the ones produced from the other emulsification methods. The increased size of this sample can be explained by the presence of agglomerates, as can be observed in the respective micrograph in Fig. 4, which affects the volume-weighted measurements like $D_{4,3}$. Indeed, the parameter D_{50} showed a smaller difference when was compared to the other samples.

Regarding resveratrol retention, a sharp difference could be noticed between the microparticles obtained from the three emulsification methods. A resveratrol amount higher than what was expected was found in the powder from the “batch system” emulsions. It indicates that the combination of the disk membrane emulsification to the spray drying process did not cause losses of resveratrol. With respect to the higher concentration than the one originally added to the formulations ($\sim 135\%$), one possibility is that part of the carrier material could have been lost within the atomizer during the drying process (Maschke et al., 2007). As for the microparticles obtained from the sonicated emulsions, resveratrol losses around 10% were observed, which indicates a good capacity for the retention of the compound. Conversely, the microparticles obtained from the “continuous system” emulsions presented a very low resveratrol retention ($\sim 15\%$). This result is very contrasted to what was expected for the process, since it is gentler and presents very low temperature increase, which represents more propitious conditions for resveratrol preservation.

Despite the difference on the resveratrol retention of the spray-dried microparticles, the encapsulation efficiency showed not to be dependent upon the emulsification process, since the three powdered samples had similar values (93%–97%). In this case, the three emulsification processes were able to promote the entrapment of resveratrol within the

particles once the emulsions were dried.

Particles water content presented similar values ($\sim 3\%$) independent of the emulsification process. Since the formulations were the same used for the three processes, it shows that the spray drying process tends to dominate over samples humidity rather than the emulsification process.

3.3.3. Reconstituted emulsions

The ability of an emulsion on preserving the original characteristics of droplet size and size distribution after submitted to spray drying can be evaluated by resuspending the powder in water for emulsions reconstitution (Drapala et al., 2017). Size parameters and micrographs of spray-dried powders after reconstitution are shown in Table 3 and Fig. 4, respectively. The sonicated emulsions were able to keep their size characteristics after undergoing the spray drying process, as evidenced both by the mean diameter and by the micrographs. On the other hand, the “batch system” and the “continuous system” emulsions showed an intense decrease on D_{50} after submitted to the atomization process. This reduction was probably caused by the pressure at which the atomizing air was forced through the nozzle, which seems sufficient to cause deformation and disruption of the oil droplets. This same pressure apparently could not affect the droplets of the sonicated emulsions, which had a much smaller mean diameter. The droplet size range reached by the ultrasound process has apparently provided increased stability to the emulsions, hence droplets were less susceptible to the effects of the atomizing air pressure and were able to keep their original size after the spray drying process.

Despite the droplet reduction caused by the atomization, the “batch system” particles were able to keep the same amount of resveratrol initially added to the formulation, as mentioned in section 3.3.2. As for

Table 3
Size parameters of emulsions and spray-dried microparticles, and resveratrol retention results for microparticles.

Sample	Emulsification process	Energy density (MJm ⁻³)	D _{4,3} (µm)	D ₁₀ (µm)	D ₅₀ (µm)	D ₉₀ (µm)	Span (dimensionless)	Water content (%)	Resveratrol retention (%)	Encapsulation efficiency (%)	Resveratrol loading (mg RSV/g of powder)
RSV-loaded emulsions	Batch system	56.91	52.30 ± 1.70 ^b	30.65 ± 0.05 ^c	52.11 ± 1.67 ^b	74.45 ± 3.02 ^b	0.84 ± 0.03 ^a	–	–	–	–
	Ultrasound	800.00	0.22 ± 0.01 ^a	0.07 ± 0.00 ^a	0.16 ± 0.01 ^a	0.45 ± 0.01 ^a	2.31 ± 0.02 ^b	–	–	–	–
	Continuous system	314.70	74.21 ± 9.34 ^b	13.49 ± 0.41 ^b	63.23 ± 5.93 ^b	150.82 ± 25.37 ^c	2.16 ± 0.21 ^b	–	–	–	–
Spray-dried particles	Batch system	56.91	22.88 ± 0.24 ^b	4.07 ± 0.41 ^a	14.71 ± 0.37 ^b	42.86 ± 0.95 ^b	2.64 ± 0.16 ^b	2.64 ± 0.11 ^a	135.08 ± 9.33 ^c	97.98 ± 0.06 ^a	0.90 ± 0.05 ^c
	Ultrasound	800.00	12.78 ± 1.02 ^a	3.19 ± 0.33 ^a	10.28 ± 0.20 ^a	22.44 ± 1.12 ^a	1.88 ± 0.18 ^a	2.79 ± 0.17 ^a	89.23 ± 5.19 ^b	97.37 ± 0.34 ^a	0.60 ± 0.03 ^b
	Continuous system	314.70	14.43 ± 0.11 ^a	3.87 ± 0.65 ^a	11.17 ± 0.93 ^a	25.13 ± 1.10 ^a	1.91 ± 0.12 ^a	3.07 ± 0.18 ^a	15.33 ± 8.17 ^a	93.88 ± 3.54 ^a	0.10 ± 0.04 ^a
Reconstituted emulsions	Batch system	56.91	8.44 ± 0.80 ^b	1.42 ± 0.09 ^c	6.55 ± 0.34 ^c	17.50 ± 0.34 ^b	2.45 ± 0.06 ^a	–	–	–	–
	Ultrasound	800.00	0.24 ± 0.01 ^a	0.08 ± 0.00 ^a	0.17 ± 0.01 ^a	0.51 ± 0.01 ^a	2.60 ± 0.03 ^a	–	–	–	–
	Continuous system	314.70	12.46 ± 1.59 ^b	1.11 ± 0.02 ^b	4.22 ± 0.27 ^b	24.71 ± 0.69 ^c	5.59 ± 0.50 ^b	–	–	–	–

RSV: resveratrol; Different lowercase letters in the same column represent statistically significant difference ($p < 0.05$) between the same type of sample (RSV-loaded emulsion, spray-dried particles or reconstituted emulsions) and different processes (dispersion cell, sonication, torsional system).

the “continuous system” samples, the droplet disruption is another factor to be considered regarding the lower resveratrol retention. Such disruption could have expelled the compound from the oil phase, and its exposure to the high temperature of the spray drying process could have damaged its preservation.

3.3.4. Energy density

Process optimization and scaling up are good reasons for the relevance of energy density evaluation in emulsification processes (Schubert and Engel, 2004). As shown in Table 3, membrane emulsification using the “batch system” was the process with the lowest energy density demand (~57 MJm⁻³), followed by the “continuous system” (~315 MJm⁻³) and the ultrasound (800 MJm⁻³). These calculations are in accordance with those obtained in the works by Holdich et al. (2020) and Yu et al. (2022) where the authors presented a comparison between the power requirement of the membrane emulsification process and other conventional systems. They concluded that, to obtain droplets of similar size, membrane emulsification requires approximately two orders of magnitude less than other techniques. To manufacture smaller droplets in the membrane systems, as per Equation (1), swap to the membrane with the smaller pore size would be needed, or viscosity of the continuous phase could be increased. This change would not modify the energy requirements as the resistance of the membranes with the straight through pores is negligible (Kosvintsev et al., 2005) compared to nylon and ceramic interconnected pores (Yu et al., 2022).

Membrane emulsification is known as a “made-to-measure” system where the droplets are formed individually and the control over the size is usually higher, leading to the formation of monodispersed emulsions. Such methods generally apply lower shear stresses over the samples hence have small increase in temperature, which enable their use also for heat sensitive materials processing (Spyropoulos et al., 2011). Since lower shear stresses are required, the energy demanded for the process is also reduced, and therefore the made-to-measure systems are also classified as low energy methods for emulsions production. Conversely,

the ultrasound emulsification is based on the droplet disruption caused by the acoustic cavitation phenomenon, by which the droplets of the coarse emulsion obtained using the rotor-stator device are sequentially reduced as far as the sonication is applied to the sample, which demands high energy input to cause droplet disruption. Ultrasound emulsification could be used to manufacture larger droplets if the sonication is run for shorter periods as reported by other authors (Yu et al., 2022; Taha et al., 2020; Consoli et al., 2017), however in this case broader droplet size is observed.

An interesting finding here is that the spray drying of the “batch system” emulsions produced particles of excellent resveratrol retention and encapsulation efficiency, even though their mean droplet size was significantly higher than those of the sonicated emulsions. The “continuous system” process also required lower energy density in comparison to the ultrasound process, and was able to reach high encapsulation efficiency (~94%) though with low resveratrol retention (~15%) probably due to the turbulent mixing within the membrane module.

These findings show that the production of powders with high resveratrol retention, encapsulation efficiency and physicochemical properties, can be achieved when membrane systems are combined with spray drying even though larger drops were produced by the membrane system.

4. Conclusions

Our work evaluated the production of resveratrol-loaded emulsions and their spray-dried microparticles, focusing on the property characterization when different emulsification processes were used. Results gave an interesting perspective for the comparison between membrane and sonication processes, as high encapsulation efficiencies were obtained for both, despite the larger droplet diameter and lower energy requirements presented by the membrane emulsification process. No cooling of the emulsion was needed during the “batch” and “continuous”

membrane emulsification process while the ice bath was needed to maintain the temperature with the ultrasound emulsion. In this sense, the “batch system” membrane emulsification process is proposed as an efficient alternative for the microencapsulation of resveratrol, with low energy consumption, which is quite interesting for scaling-up processes. Future studies are needed to obtain improved results regarding resveratrol retention using pilot scale for membrane emulsification and continuous high throughput systems developed by Holdich et al. (2020) which have less turbulence compared to Torsional system will be tested.

Credit author statement

Larissa Consoli: Conceptualization, Investigation, Formal analysis, Data curation, Writing – original draft, Visualization. *Míriam D. Hubinger*: Supervision, Writing – review and editing, Funding acquisition. *Marijana M. Dragosavac*: Conceptualization, Methodology, Resources, Supervision, Writing – review and editing, Funding acquisition.

Declaration of competing interest

The authors declare that they have no known competing financial interests or personal relationships that could have appeared to influence the work reported in this paper.

Data availability

Data will be made available on request.

Acknowledgments

The authors are grateful to the Chemical Engineering Department of Loughborough University for the use of the laboratories and equipment. Funding: This study was financed in part by the Coordenação de Aperfeiçoamento de Pessoal de Nível Superior–Brasil (CAPES) – Código de financiamento 001, and by Fapesp (2015/11984–7) and CNPq (140273/2014–0).

Appendix A. Supplementary data

Supplementary data to this article can be found online at <https://doi.org/10.1016/j.jfoodeng.2023.111488>.

References

- AOAC, 2005. *Official Methods of Analysis of AOAC*.
- Assadpour, E., Jafari, S.M., 2019. Advances in spray-drying encapsulation of food bioactive ingredients: from microcapsules to nanocapsules. *Annu. Rev. Food Sci. Technol.* 10, 103–131. <https://doi.org/10.1146/annurev-food-032818-121641>.
- Consoli, L., de Figueiredo Furtado, G., da Cunha, R.L., Hubinger, M.D., 2017. High solids emulsions produced by ultrasound as a function of energy density. *Ultrason. Sonochem.* 38, 772–782. <https://doi.org/10.1016/j.ultsonch.2016.11.038>.
- Consoli, L., Dias, R.A.O., da Silva Carvalho, A.G., da Silva, V.M., Hubinger, M.D., 2019. Resveratrol-loaded microparticles: assessing Maillard conjugates as encapsulating matrices. *Powder Technol.* 353, 247–256. <https://doi.org/10.1016/j.powtec.2019.04.085>.
- Consoli, L., Hubinger, M.D., Dragosavac, M.M., 2020. Encapsulation of resveratrol using Maillard conjugates and membrane emulsification. *Food Res. Int.* 137, 109359 <https://doi.org/10.1016/j.foodres.2020.109359>.
- Dragosavac, M.M., Sovilj, M.N., Kosvintsev, S.R., Holdich, R.G., Vladislavjević, G.T., 2008. Controlled production of oil-in-water emulsions containing unrefined pumpkin seed oil using stirred cell membrane emulsification. *J. Membr. Sci.* 322, 178–188. <https://doi.org/10.1016/j.memsci.2008.05.026>.
- Drapala, K.P., Auty, M.A.E., Mulvihill, D.M., O'Mahony, J.A., 2017. Influence of emulsifier type on the spray-drying properties of model infant formula emulsions. *Food Hydrocolloids* 69, 56–66. <https://doi.org/10.1016/j.foodhyd.2016.12.024>.
- Drusch, S., Berg, S., Scampicchio, M., Serfert, Y., Somoza, V., Mannino, S., Schwarz, K., 2009. Role of glycated caseinate in stabilisation of microencapsulated lipophilic functional ingredients. *Food Hydrocolloids* 23, 942–948. <https://doi.org/10.1016/j.foodhyd.2008.07.004>.
- Holdich, R., Dragosavac, M., Williams, B., Trotter, S., 2020. High throughput membrane emulsification using a single-pass annular flow crossflow membrane. *AIChE J.* 66 <https://doi.org/10.1002/aic.16958>.
- Jafari, S.M., He, Y.H., Bhandari, B., 2007. Production of sub-micron emulsions by ultrasound and microfluidization techniques. *J. Food Eng.* 82, 478–488. <https://doi.org/10.1016/j.jfoodeng.2007.03.007>.
- Karbstein, H., Schubert, H., 1995. Developments in the continuous mechanical production of oil-in-water macro-emulsions. *Chem. Eng. Process* 34, 205–211. [https://doi.org/10.1016/0255-2701\(94\)04005-2](https://doi.org/10.1016/0255-2701(94)04005-2).
- Kosvintsev, S.R., Gasparini, G., Holdich, R.G., Cumming, I.W., Stillwell, M.T., 2005. Liquid–Liquid membrane dispersion in a stirred cell with and without controlled shear. *Ind. Eng. Chem. Res.* 44, 9323–9330. <https://doi.org/10.1021/ie0504699>.
- Li, J., Mao, H., Kawazoe, N., Chen, G., 2017. Insight into the interactions between nanoparticles and cells. *Biomater. Sci.* 5, 173–189. <https://doi.org/10.1039/C6BM00714G>.
- Maschke, A., Becker, C., Eyrich, D., Kiermaier, J., Blunk, T., Gopferich, A., 2007. Development of a spray congealing process for the preparation of insulin-loaded lipid microparticles and characterization thereof. *Eur. J. Pharm. Biopharm.* 65, 175–187. <https://doi.org/10.1016/j.ejpb.2006.08.008>.
- Pereira, M.M., Raposo, N.R.B., Brayner, R., Teixeira, E.M., Oliveira, V., Quintão, C.C.R., Camargo, L.S.A., Mattoso, L.H.C., Brandão, H.M., 2013. Cytotoxicity and expression of genes involved in the cellular stress response and apoptosis in mammalian fibroblast exposed to cotton cellulose nanofibers. *Nanotechnology* 24. <https://doi.org/10.1088/0957-4484/24/7/075103>.
- Salama, A.H., 2020. Spray drying as an advantageous strategy for enhancing pharmaceuticals bioavailability. *Drug Deliv. Transl. Res.* <https://doi.org/10.1007/s13346-019-00648-9>.
- Santos, A.C., Pereira, I., Pereira-Silva, M., Ferreira, L., Caldas, M., Magalhães, M., Figueiras, A., Ribeiro, A.J., Veiga, F., 2019. Nanocarriers for resveratrol delivery: impact on stability and solubility concerns. *Trends Food Sci. Technol.* 91, 483–497. <https://doi.org/10.1016/j.tifs.2019.07.048>.
- Santos, T.P., Cunha, R.L., 2020. Designing biotechnological processes to reduce emulsions formation and improve oil recovery: study of antifoams application. *Biochem. Eng. J.* 163, 107745 <https://doi.org/10.1016/j.bej.2020.107745>.
- Schubert, H., Engel, R., 2004. Product and formulation engineering of emulsions. *Chem. Eng. Res. Des.* 82, 1137–1143. <https://doi.org/10.1205/cerd.82.9.1137.44154>.
- Silva, P.S., Dragosavac, M.M., Vladislavjević, G.T., Bandulasena, H.C.H., Holdich, R.G., Stillwell, M., Williams, B., 2015. Azimuthally oscillating membrane emulsification for controlled droplet production. *AIChE J.* 61, 3607–3615. <https://doi.org/10.1002/aic.14894>.
- Sneha, K., Kumar, A., 2022. Nanoemulsions: techniques for the preparation and the recent advances in their food applications. *Innovat. Food Sci. Emerg. Technol.* 76, 102914 <https://doi.org/10.1016/j.ifset.2021.102914>.
- Spyropoulos, F., Hancock, R.D., Norton, I.T., 2011. Food-grade emulsions prepared by membrane emulsification techniques. *Procedia Food Sci.* 1, 920–926. <https://doi.org/10.1016/j.profoo.2011.09.139>.
- Taha, A., Ahmed, E., Ismaiel, A., Ashokkumar, M., Xu, X., Pan, S., Hu, H., 2020. Ultrasonic emulsification: an overview on the preparation of different emulsifiers-stabilized emulsions. *Trends Food Sci. Technol.* 105, 363–377. <https://doi.org/10.1016/j.tifs.2020.09.024>.
- Tibolla, H., Pelissari, F.M., Martins, J.T., Vicente, A.A., Menegalli, F.C., 2018. Cellulose nanofibers produced from banana peel by chemical and mechanical treatments: characterization and cytotoxicity assessment. *Food Hydrocolloids* 75, 192–201. <https://doi.org/10.1016/j.foodhyd.2017.08.027>.
- Vladislavjević, G.T., Williams, R.A., 2005. Recent developments in manufacturing emulsions and particulate products using membranes. *Adv. Colloid Interface Sci.* 113, 1. <https://doi.org/10.1016/j.cis.2004.10.002>, 20.
- Yu, S., Jing, Y., Fan, Y., Xiong, L., Wang, H., Lei, J., Zhang, Y., Liu, J., Wang, S., Chen, X., Sun, H., 2022. Ultrahigh efficient emulsification with drag-reducing liquid gating interfacial behavior. *Proc. Natl. Acad. Sci. USA* 119 (29). <https://doi.org/10.1073/pnas.2206462119> e2206462119.
- Zhang, Q., Zhou, Y., Yue, W., Qin, W., Dong, H., Vasanthan, T., 2021. Nanostructures of protein-polysaccharide complexes or conjugates for encapsulation of bioactive compounds. *Trends Food Sci. Technol.* 109, 169–196. <https://doi.org/10.1016/j.tifs.2021.01.026>.